BCSIR

Available online at www.banglajol.info

Bangladesh J. Sci. Ind. Res. **48(1)**, 59-70, 2013

BANGLADESH JOURNAL OF SCIENTIFIC AND INDUSTRIAL RESEARCH

E-mail: bjsir07@gmail.com

Bifurcation study of thermal flows through a rotating curved square duct

R. N. Mondal[1*], A. K. Datta[2] and B. Mondal[3]

[a]*Mathematics Discipline; Science, Engineering and Technology School, Khulna University, Khulna-9208, Bangladesh*

[b]*Dept. of Mathematics, The University of Asia Pacific, Dhanmondi, Dhaka*

[c]*Dept. of Mathematics, Govt. M. M. City College, Khulna*

Abstract

In this paper, a comprehensive numerical study is presented for the fully developed thermal flows through a rotating curved duct with square cross section. Numerical calculations are carried out over a wide range of the Taylor number $0 \le Tr \le 3000$ for two cases of the Dean numbers, $Dn = 1000$ and $Dn = 2000$. A temperature difference is applied across the vertical sidewalls for the Grashof number $Gr = 500$, where the outer wall is heated and the inner wall cooled. Spectral method is used as a basic tool to solve the system of non-linear differential equations. The rotation of the duct about the center of curvature is imposed, and the effects of rotation (*Coriolis force*) on the flow characteristics are investigated. As a result, multiple branches of asymmetric steady solutions with two-, three- and four-vortex solutions are obtained. Linear stability of the steady solutions is also investigated.

Keyword: Rotating curved duct, Secondary flow, Dean number, Taylor number.

Introduction

The study of flows and heat transfer through curved ducts and channels is of fundamental interest because of its practical application in chemical, mechanical and biological engineering. Due to engineering application and their intricacy, flow in a rotating curved duct has become one of the most challenging research fields of fluid mechanics. A quantitative analogy between flows in stationary curved pipes and orthogonally rotating straight pipes has been reported by Ishigaki (1993, 1996). Taking this analogy as a basis, this study describes the characteristics of more general and complicated flow in rotating curved ducts, which are relevant to systems involving helically or spirally coiled pipes rotating about the coil axis. Such rotating flow passages are used in cooling systems in rotating machinery. The flow systems are also encountered in separation processes; scientists have paid considerable attention in order to study the characteristics of the flows in these rotating systems. The present work is on the fully developed bifurcation structure of the forced convection in a tightly coiled duct of square cross-section. The flow geometry is illustrated in Fig. 1. A viscous fluid is driven by a streamwise pressure gradient to flow through a square duct with a streamwise curvature and a uniform wall heat flux.

Such flows and transport phenomena are the subject of intense investigations due to its intrinsic interest and its relevance to a host of areas involving curved passages and surfaces from piping systems for various fluids to blood flows in the human arterial system (Wang and Yang, 2004; Wang and Liu, 2007a).

The forced convection in a curved duct of square cross-section is characterized by the three dimensionless governing parameters: one geometrical parameter δ (the curvature ratio defined by l/L, the ratio of duct width l over the radius of curvature L (Fig. 1), one thermophysical parameter Pr (the Prandtl number) and one dynamical parameter Dn, the Dean number. The fully developed bifurcation structure of the forced convection in loosely coiled ducts has been well studied in low Dean number region [Winters, 1987; Daskopoulos and Lenhoff, 1989]. The readers are referred to (Yang and Wang, 2003; Mondal *et. al.*, 2007) for the effects of rotation-induced Coriolis force and buoyancy force on flow multiplicity in loosely coiled ducts. The location of limit and bifurcation points was found to be insensitive to δ for curvature ratios less than 0.1, but at higher curvature ratios, they move to higher

* Corresponding author. email: rnmondal71@yahoo.com

Dean numbers (Winters, 1987). Upon increasing the Dean number, a richer bifurcation structure with new limit/bifurcation points, solution branches and complicated flow structures is obtained (Wang and Liu, 2007b) because of the stronger non-linearity of the problem. Because of the lack of solution structures in high Dean number region, there is a long-standing controversy over solutions obtained by different methods without considering the multiplicity. The present work is, therefore, a relatively comprehensive study on the bifurcation structure for the laminar forced convection in a rotating curved duct of square cross-section in a high Dean number region, because it has practical applications in metallic industry, gas turbines, electric generators/motors etc.

One of the interesting phenomena of the flow through a curved duct is the bifurcation of the flow because generally there exist many steady solutions due to channel curvature. Many researches have performed experimental and numerical investigation on developing and fully developed curved duct flows. An early complete bifurcation study of two-dimensional (2-D) flow through a curved duct with square cross section was performed by Winters (1987). However an extensive treatment of the flow through a curved square duct was performed by Mondal (2006). He found a close relationship between the unsteady solutions and the bifurcation diagram of steady solutions. Ishigaki (1996) examined the flow structure and friction factor numerically for both the counter-rotating and co-rotating curved circular pipe with a small curvature. Zhang *et al.* (2001) examined the flow in a rotating curved annular pipe and found an eight-cell phenomenon of the secondary flow. Selmi *et al.* (1994) examined the combined effects of system rotation and curvature on the bifurcation structure of two-dimensional flows in a rotating curved duct with square cross section. Wang and Cheng (1996), employing finite volume method, examined the flow characteristics and heat transfer in curved square ducts for positive rotation and found reverse secondary flow for the co-rotation cases. Selmi and Nandukumer (1999) and Yamamoto *et al.* (1999) performed the studies on the flow characteristics in rotating curved rectangular ducts. Yamamoto *et al.* (1999), employing the spectral method, examined the flow structure and the flow rate ratio for the flow in a rotating curved square duct and found a six-cell phenomenon of the secondary flow. Zhang *et al.* (2001) investigated the combined effects of the Coriolis force and the centrifugal force on the flows in rotating curved rectangular ducts numerically. Yang and Wang (2003) performed comprehensive numerical study on bifurcation structure and stability of solutions for laminar mixed convection in a rotating curved duct of square cross section.

It is well known that, the fluid flowing in a rotating curved duct is subjected to two forces: the Corlis force, caused by the rotation of the duct, and centrifugal force caused by the curvature of the duct. These two forces affect each other, as a result complex behavior of the secondary flow and the axial flow can be obtained. For isothermal flows of a constant property fluid, the Coriolis force tends to produce vorticity while centrifugal force is purely hydrostatic. When a temperature induced variation of fluid density occurs for non-isothermal flows, both Coriolis and centrifugal type buoyancy forces can contribute to the generation of vorticity (Mondal *et. al.*, 2007). These two effects of rotation either enhance or counteract each other in a non-linear manner depending on the direction of wall heat flux and the flow domain. Therefore, the effect of the rotation of the system is more subtle and complicated and yields new; richer features of flow and heat trahsfer in general, bifurcation and stability in particular, for non-isothermal flows. Recently, Mondal *et al.* (2007) performed numerical prediction of the non-isothermal flows through a rotating curved square duct and revealed some of such new features. They performed numerical investigation of the flows with a temperature difference between the vertical sidewalls for small Grashof number ($Gr = 100$) and obtained multiple branches of solutions. However, there is no known study on bifurcation and stability for forced convection in a rotating curved duct with square cross section for large Grashof number. The present paper is, therefore, an attempt to fill up this gap with the study of the flow characteristics through a rotating curved square duct with differentially heated vertical sidewalls for large Grashof number.

In the present paper, a comprehensive numerical study is presented for fully developed two-dimensional flow of viscous incompressible fluid through a rotating curved square duct. Flow characteristics are investigated over a wide range of the Taylor number $0 \le Tr \le 3000$ for two cases of the Dean numbers, $Dn = 1000$ and $Dn = 2000$. Studying the effects of rotation on the flow characteristics is an important objective of the present study.

Governing Equations

Consider a hydrodynamically and thermally fully developed two-dimensional flow of viscous incompressible fluid through a rotating curved square duct, whose height and width are $2h$ and $2l$, respectively. In the present case, $h = l$. Figure 1 shows the coordinate system with relevant notations, where C is the center of the duct cross-section and L is the radius of curvature of the duct. The x' and y' axes are taken to be in the horizontal and vertical directions

respectively, and z' is the coordinate along the center-line of the duct, i.e., the axial direction. The system rotates at a constant angular velocity Ω_T around the y' axis. It is assumed that the outer wall of the duct is heated while the inner one is cooled. The temperature of the outer wall is $T_0 + \Delta T$ and that of the inner wall is $T_0 - \Delta T$, where $\Delta T > 0$. It is also assumed that the flow is uniform in the axial direction, and that it is driven by a constant pressure gradient $G\left(G = \frac{-\partial P'}{\partial z'}\right)$ along the centre-line of the duct. Then the continuity, Navier-Stokes and energy equations, in terms of dimensional variables, are expressed as:

Continuity equation:

$$\frac{\partial u'}{\partial r'} + \frac{\partial v'}{\partial y'} + \frac{u'}{r'} = 0 \tag{1}$$

Momentum equations:

$$\frac{\partial u'}{\partial t'} + u'\frac{\partial u'}{\partial r'} + v'\frac{\partial u'}{\partial y'} - \frac{w'^2}{r'} - 2\Omega_T w' = -\frac{1}{\rho}\frac{\partial P'}{\partial r'} + \nu\left[\frac{\partial^2 u'}{\partial r'^2} + \frac{\partial^2 u'}{\partial y'^2} + \frac{1}{r'}\frac{\partial u'}{\partial r'} - \frac{u'}{r'^2}\right] \tag{2}$$

$$\frac{\partial v'}{\partial t'} + u'\frac{\partial v'}{\partial r'} + v'\frac{\partial v'}{\partial y'} - \frac{w'^2}{r'} = -\frac{1}{\rho}\frac{\partial P'}{\partial r'} + \nu\left[\frac{\partial^2 v'}{\partial r'^2} + \frac{1}{r'}\frac{\partial v'}{\partial r'} + \frac{\partial^2 v'}{\partial y'^2}\right] + g\beta T' \tag{3}$$

$$\frac{\partial w'}{\partial t'} + u'\frac{\partial w'}{\partial r'} + v'\frac{\partial w'}{\partial y'} + \frac{u'w'}{r'} + 2\Omega_T u' = -\frac{1}{\rho r'}\frac{\partial P'}{\partial z'} + \nu\left[\frac{\partial^2 w'}{\partial r'^2} + \frac{\partial^2 w'}{\partial y'^2} + \frac{1}{r'}\frac{\partial w'}{\partial r'} - \frac{w'}{r'^2}\right] \tag{4}$$

Energy equation:

$$\frac{\partial T'}{\partial t'} + u'\frac{\partial T'}{\partial r'} + v'\frac{\partial T'}{\partial y'} = \kappa\left[\frac{\partial^2 T'}{\partial r'^2} + \frac{1}{r'}\frac{\partial T'}{\partial r'} + \frac{\partial^2 T'}{\partial y'^2}\right] \tag{5}$$

Where, $r' = L = x'$, and u', v' and w' are the dimensional velocity components in the x', y' and z' directions respectively, and these velocities are zero at the wall. Here P' is the dimensional pressure, T' is the dimensional temperature and t' is the dimensional time. In the above formulations, ρ, υ, β, κ and g are the density, the kinematic viscosity, the coefficient of thermal expansion, the coefficient of thermal diffusivity and the gravitational acceleration, respectively. Thus, in Eq. (1) to (5) the variables with prime denote the dimensional quantities. The dimensional variables are non-dimensionalized by using the representative length l and the representative velocity $U_0 = \frac{\upsilon}{l}$. We introduce the non-dimensional variables defined as:

$$u = \frac{u'}{U_0}, \quad v = \frac{v'}{U_0}, \quad w = \frac{\sqrt{2\delta}}{U_0} w',$$

$$x = \left(\frac{x'}{l} - \frac{1}{\delta}\right), \quad \bar{y} = \frac{y'}{l}, \quad z = \frac{z'}{l}$$

$$T = \frac{T'}{\Delta T'}, \quad t = \frac{U_0}{d}t', \quad \delta = \frac{l}{L}, \quad P = \frac{P'}{\rho {U_0}^2}$$

Where, u, v and w are the non-dimensional velocity components in the $x, \bar{y}$ and z directions, respectively; t is the non-dimensional time, P is the non-dimensional pressure, δ is the non-dimensional curvature defined as $\delta = \frac{l}{L}$, and temperature is nondimensionalized by ΔT. Henceforth, all the variables are nondimensionalized if not specified.

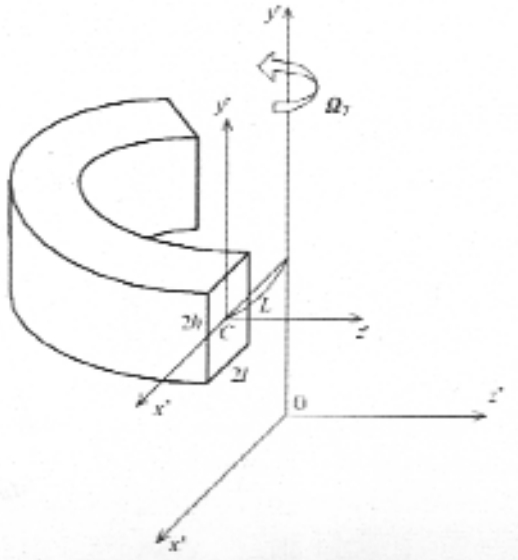

Fig. 1. Coordinate system of the rotating curved duct

Since the flow field is uniform in the z direction, the sectional stream function ψ is introduced as

$$u = \frac{1}{1+\delta x}\frac{\partial \psi}{\partial y}, \quad v = -\frac{1}{1+\delta x}\frac{\partial \psi}{\partial x} \tag{6}$$

Then, the basic equations for the axial velocity w, the stream function ψ and temperature T are expressed in terms of non-dimensional variables with the *Boussinesq approximation* as

$$\left(1+\delta x\right)\frac{\partial w}{\partial t}+\frac{\partial(w,\psi)}{\partial(x,y)}-Dn+\frac{\delta^2 w}{1+\delta x}=$$
$$(1+\delta x)\Delta_2 w-\frac{\delta}{1+\delta x}\frac{\partial \psi}{\partial y}w+\delta\frac{\partial w}{\partial x}-$$
$$\delta Tr\frac{\partial \psi}{\partial y} \tag{7}$$

$$\left(\Lambda_2-\frac{\delta}{1+\delta x}\frac{\partial}{\partial x}\right)\frac{\partial \psi}{\partial t}=-\frac{1}{(1+\delta x)}\frac{\partial(\Delta_2\psi,\psi)}{\partial(x,y)}+$$
$$\frac{\delta}{(1+\delta x)^2}\left[\frac{\partial \psi}{\partial y}\left(2\Delta_2\psi-\frac{3\delta}{1+\delta x}\frac{\partial \psi}{\partial x}+\frac{\partial^2\psi}{\partial x^2}\right)\right.$$
$$\left.-\frac{\partial \psi}{\partial x}\frac{\partial^2\psi}{\partial x\partial y}\right]+\frac{\delta}{(1+\delta x)^2}\left[3\delta\frac{\partial^2\psi}{\partial x^2}-\frac{3\delta^2}{1+\delta x}\frac{\partial \psi}{\partial x}\right]$$
$$-\frac{2\delta}{1+\delta x}\frac{\partial}{\partial x}\Delta_2\psi+w\frac{\partial w}{\partial y}+\Delta_2{}^2\psi-G_r(1+\delta x)\frac{\partial T}{\partial x}$$
$$+\frac{1}{2}Tr\frac{\partial w}{\partial y}, \tag{8}$$

$$\frac{\partial T}{\partial t}+\frac{1}{(1+\delta x)}\frac{\partial(T,\psi)}{\partial(x,y)}=\frac{1}{\Pr}\left(\Delta_2 T+\frac{\delta}{1+\delta x}\frac{\partial T}{\partial x}\right) \tag{9}$$

where,

$$\Lambda_2=\frac{\partial^2}{\partial x^2}+\frac{\partial^2}{\partial y^2}, \quad \frac{\partial(f,g)}{\partial(x,y)}=\frac{\partial f}{\partial x}\frac{\partial g}{\partial y}-\frac{\partial f}{\partial y}\frac{\partial g}{\partial x} \tag{10}$$

The non-dimensional parameters Dn, the Dean number, Gr, the Grashof number, Tr, the Taylor number and $\Pr$, the Prandtl number, which appear in equation (7) and (8) are defined as:

$$Dn=\frac{Gl^3}{\mu\upsilon}\sqrt{\frac{2l}{L}}, \quad Gr=\frac{\beta g\Delta T\ l^3}{\upsilon^2}$$
$$Tr=\frac{2\sqrt{2\delta}\ \ \Omega_T l^3}{\upsilon\delta}, \quad \Pr=\frac{\upsilon}{\kappa} \tag{11}$$

where, μ is the viscosity of the fluid. In the present study, only Dn and Tr are varied, while δ, Gr and $\Pr$ are fixed as $\delta=0.1$, $Gr=500$ and $\Pr=7.0$ for water.

The rigid boundary conditions for w and ψ are used as:

$$w(\pm1,y)=w(x,\pm1)=\psi(\pm1,y)=$$
$$\psi(x,\pm1)=\frac{\partial \psi}{\partial x}(\pm1,y)=\frac{\partial \psi}{\partial y}(x,\pm1)=0 \tag{12}$$

and the temperature T is assumed to be constant on the walls as:

$$T(1,y)=1,\ T(-1,y)=-1, T(x,\pm1)=x \tag{13}$$

There is a class of solutions which satisfy the following symmetry condition with respect to the horizontal plane $y=0$:

$$\left.\begin{aligned}(x,y,t)&\Rightarrow w(x,-y,t),\\ \psi(x,y,t)&\Rightarrow -\psi(x,-y,t),\\ T(x,y,t)&\Rightarrow -T(x,-y,t)\end{aligned}\right\} \tag{14}$$

The solution which satisfies the condition (14) is called a symmetric solution, and that which does not an asymmetric solution. It should be noted that Eqs. (7), (8) and (9) are invariant under the transformation of the variables

$$\left.\begin{aligned}y&\Rightarrow -y\\ w(x,y,t)&\Rightarrow w(x,-y,t),\\ \psi(x,y,t)&\Rightarrow -\psi(x,-y,t),\\ T(x,y,t)&\Rightarrow -T(x,-y,t)\end{aligned}\right\} \tag{15}$$

Therefore, the case of heating the inner sidewall and cooling the outer sidewall can be deduced directly from the results obtained in this study. Equations (7) – (9) would serve as the basic governing equations which are solved numerically as discussed in the following section.

Numerical Calculations

In order to solve the Eqs. (7) to (9) numerically, the spectral method is used. This is the method which is thought to be the best numerical method for solving the Navier-Stokes as well as energy equations (Gottlieb and Orszag, 1977). By this method the variables are expanded in a series of

functions consisting of Chebyshev polynomials. That is, the expansion functions $\phi_n(x)$ and $\psi_n(x)$ are expressed as

$$\left.\begin{aligned}\varphi_n(x) &= (1-x^2)\,C_n(x),\\ \psi_n(x) &= (1-x^2)^2 C_n(x)\end{aligned}\right\} \tag{16}$$

where $C_n(x) = \cos(n\cos^{-1}(x))$ is the n^{th} order Chebyshev polynomial. $w(x,y,t)$, $\psi(x,y,t)$ and $T(x,y,t)$ are expanded in terms of the expansion functions $\phi_n(x)$ and $\psi_n(x)$ as:

$$\left.\begin{aligned}w(x,y,t) &= \sum_{m=0}^{M}\sum_{n=0}^{N} w_{mn}(t)\,\phi_m(x)\,\phi_n(y)\\ \psi(x,y,t) &= \sum_{m=0}^{M}\sum_{n=0}^{N} \psi_{mn}(t)\,\psi_m(x)\,\psi_n(y).\\ T(x,,y,t) &= \sum_{m=0}^{M}\sum_{n=0}^{N} T_{mn}\,\phi_m(x)\,\phi_n(y)+x\end{aligned}\right\} \tag{17}$$

where, M and N are the truncation numbers in the x and y directions respectively, and w_{mn}, ψ_{mn} and T_{mn} are the coefficients of expansion. In order to obtain a steady solution $\overline{w}(x,y), \overline{\psi}(x,y)$ and $\overline{T}(x,y)$, the expansion series (12) is submitted into the basic Eqs. (7), (8) and (9), and the collocation method (Gottlieb and Orszag, 1977) is applied. As a result, a set of nonlinear algebraic equations for w_{mn}, ψ_{mn} and T_{mn} are obtained. The collocation points (x_i, y_j) are taken to be

$$\left.\begin{aligned}x_i &= \cos\left[\pi\left(1-\frac{i}{M+2}\right)\right], \qquad i = 1,\ldots,M+1\\ y_j &= \cos\left[\pi\left(1-\frac{j}{N+2}\right)\right], \qquad j = 1,\ldots,N+1\end{aligned}\right\} \tag{18}$$

where, $i = 1,\ldots,M+1$ and $j = 1,\ldots,N+1$. Steady solutions are obtained by the Newton-Rapshon iteration method assuming that all the variables are time independent. The convergence is assured by taking $\varepsilon_p < 10^{-10}$, where subscript p denotes the iteration number and ε_p is defined as:

$$\varepsilon_p = \sum_{m=0}^{M}\sum_{n=0}^{N}\left[\left(w_{m\,n}^{(p+1)} - w_{m\,n}^{p}\right)^2 + \left(\psi_{m\,n}^{(p+1)} - \psi_{m\,n}^{p}\right)^2 + \left(T_{m\,n}^{(p+1)} - T_{m\,n}^{p}\right)^2\right] \tag{19}$$

In the present numerical calculation, for sufficiently accuracy of the solutions, we take $M = 20$ and $N = 20$.

Linear stability of the steady solutions is investigated against two-dimensional (z independent) perturbations. To do this, the eigenvalue problem is solved, which is constructed by the application of the function expansion method, together with the collocation method, to the perturbation equations obtained from equations (7) to (9). It is assumed that the time dependence of the perturbation is $e^{\sigma t}$, where $\sigma = \sigma_r + i\sigma_i$ is the eigenvalue with σ_r the real part, σ_i the imaginary part and $i = \sqrt{-1}$. If all the real parts of the eigenvalue σ are negative, the steady solution is linearly stable, but if there exists at least one positive real part of the eigenvalue, it is linearly unstable. In the unstable region, the perturbation grows monotonically for $\sigma_i = 0$ and oscillatorily for $\sigma_i \neq 0$.

Flux through the Duct

The dimensional total flux Q' through the duct in the rotating coordinate system is calculated by:

$$Q' = \int_{-d}^{d}\int_{-d}^{d} w'\,dx'\,dy' = v\,dQ \tag{20}$$

where, $Q = \int_{-1}^{1}\int_{-1}^{1} w\,dx\,dy$ is the dimensionless total flux.

The mean axial velocity $\overline{w}'$ is expressed as

$$\overline{w}' = \frac{Qv}{4d} \tag{21}$$

In the present study, Q is used to denote the steady solution branches.

Results and discussion

We take a curved duct with square cross section and rotate it around the center of curvature with an angular velocity Ω_T. In the present study, we investigate the flow characteristics for the case of positive rotation of the duct (i.e. positive Tr), and discuss the flow phenomenon for two cases of the Dean numbers, *Case I*: $Dn = 1000$ and *Case II*: $Dn = 2000$, over a wide range of the Taylor number $0 \le Tr \le 3000$. Thus, an interesting and complicated flow behavior will be expected if the duct rotation is involved for these two cases.

Case *I*: $Dn = 1000$

Steady solutions and their linear stability analysis

By using the path continuation technique as discussed by Keller (1987), we obtain two branches of steady solutions for $Dn = 1000$. The solution branches are named the *first steady solution branch* (first branch, thin solid line) and the *second steady solution branch* (second branch, dashed line), respectively. The bifurcation structure of the two steady solution branches is shown in Fig. 2. It should be noted here that Mondal *et al.* (2006) also obtained two branches of steady solutions for the non-rotating curved square duct flows. In the following, the two steady solution branches as well as the flow patterns and temperature profiles on the respective branches are discussed.

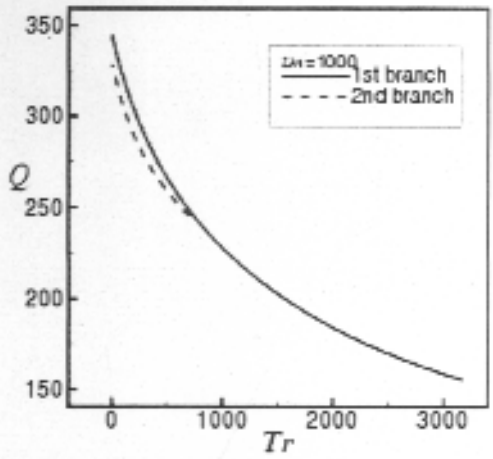

Fig. 2. Steady solution branches for $Dn = 1000$, $0 \le Tr \le 3000$ and $Gr = 500$.

The first steady solution branch

The first steady solution branch for $Dn = 1000$ is shown with a solid in Fig. 2 for $0 \le Tr \le 2000$. It should be remarked that between the two branches of steady solutions, only this branch exists throughout the whole range of Tr.

As seen in Fig. 2 the branch starts from $Tr = 0$ and extends to the direction of increasing Tr and decreasing Q ($Tr = 2000$) without any turning throughout its way. Contours of typical secondary flow and temperature profile are shown in Fig. 3 for several values of Tr on this branch. As seen in Fig. 3, the first branch is composed of two-vortex solutions. The secondary flow is an asymmetric two-vortex solution for small Tr. However as Tr increases, the asymmetry gradually disappears and the flow pattern ceases to be nearly symmetric due to weak Coriolis force. With strong centrifugal force, however, the flow pattern becomes asymmetric but as Tr increases the Coriolis force increases which balances the centrifugal force and the flow pattern becomes approximately symmetric.

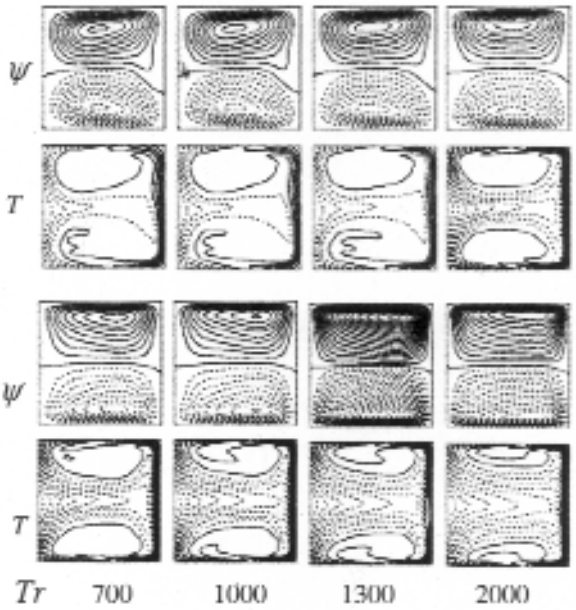

Fig. 3. Contours of secondary flow (top) and temperature profile (bottom) on the first steady solution branch at several values of Tr.

The second steady solution branch

The second steady solution branch for $Dn = 1000$, shown by a thin solid line in Fig. 2, is solely depicted in Fig. 4(a). As seen in Fig. 4(a), the branch starts from point a ($Tr = 0$) and goes to the direction of increasing Tr and decreasing Q up to point b ($Tr \le 742$), where it experiences a smooth turning and goes to the direction of increasing Q and decreasing Tr up to point c ($Tr = 0$).

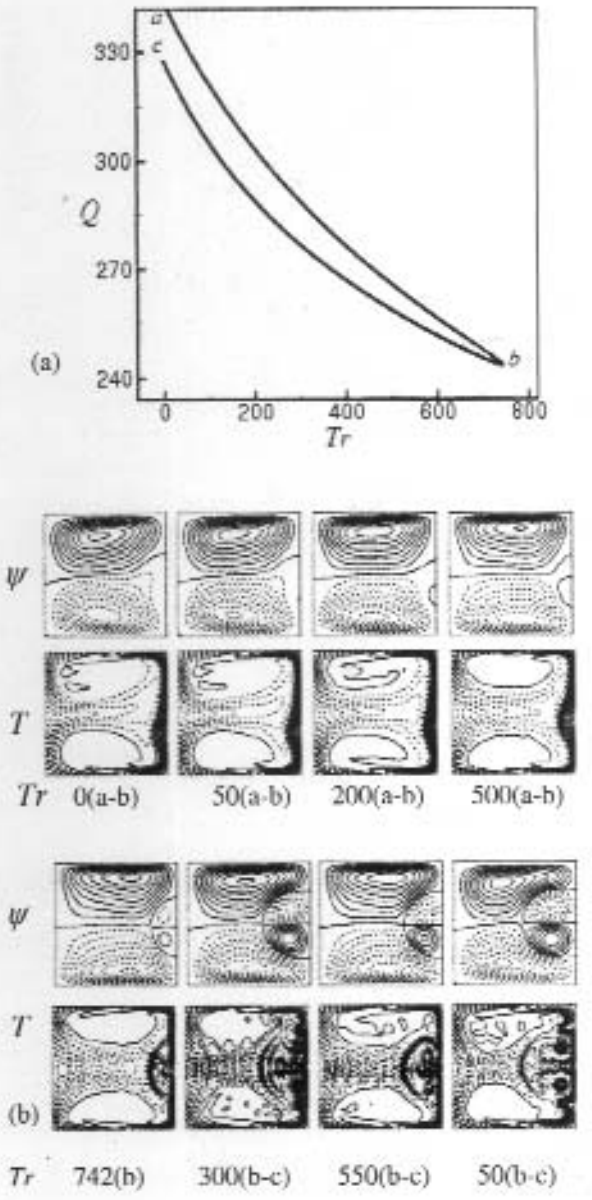

Fig. 4: (a) Second steady solution branch for $Dn = 1000$ and $Gr = 500$. (b) Contours of secondary flow (top) and temperature profile (bottom).

To observe the change of the flow patterns and temperature distributions, contours of typical secondary flow and temperature profile are shown in Fig. 4(b) for several values of Tr. As seen in Fig. 4(b), the branch is composed of asymmetric two-, three- and four-vortex solutions. It is found that on the upper part of the second branch, the secondary flow is composed of asymmetric two- and three-vortex solutions from point a to point b as Tr increases ($0 \le Tr < 742$) from 0. However, at point b, the flow becomes four-vortex solutions. On the lower part of the second branch, on the other hand, we get asymmetric four- vortex solutions (from point b to point c). In the case of temperature transmission from the outer wall (heated wall) to the fluid, it is found that the convection becomes more frequent with the increase rotation. The additional vortices, which play an important role in the enhancement of heat transfer, are called *Dean Vortices*.

Linear stability of the steady solutions for $Dn = 1000$

We investigated linear stability of the steady solutions and it is found that between the two branches of solutions, only the first steady solution branch is stable while the second branch is unstable. The first branch is partly unstable for small Tr ($Tr \le 15.3$). However, as Tr increases, the steady solution becomes stable and remains stable onwards as Tr increases. The second branch is completely unstable for any value of Tr. Thus, we find that the first steady solution is linearly stable for $15.4 \le Tr \le 2000$. The eigenvalues of the first steady solution branch are shown in Table 1, where the eigenvalues with the maximum real part of σ (first eigenvalues) are listed. Those for the linearly stable solutions are printed in bold letters. As seen in the Table 1, the stability region exists for $15.4 \le Tr \le 3000$, and the perturbation grows monotonically ($\sigma_i = 0$) for larger Tr. Therefore, the *Hopf bifurcation* occurs at $Dn = 15.4$. The region of linearly stable steady solution is shown with a thick solid line in Fig. 2.

Case II: $Dn = 2000$

Steady solutions and their linear stability analysis

We obtain four branches of steady solutions for $Dn = 2000$ and $Gr = 500$ over a wide range of Tr for $0 \le Tr \le 3000$. The bifurcation diagram of steady solutions is shown in Fig. 5. The four steady solution branches are named the *first steady solution branch* (first branch, thick solid line), the *second steady solution branch* (second branch, dashed line), the *third steady solution branch* (third branch, thin solid line) and the *fourth steady solution branch* (fourth branch, dash dotted line), respectively. The steady solution branches are obtained by the path continuation technique with various initial guesses as discussed by Mondal (2006). The branches are distinguished by the nature and number of secondary flow vortices appearing in the cross section of the duct. In this regard, it should be noted that Mondal *et al.* (2007) also obtained four braches of steady solutions for $Gr = 100$, but our result is different from theirs in the formation of solution structure.

Table I. Linear stability of first the steady solution for $Dn = 1000$ and $Gr = 500$

Tr	Q	σ_r	σ_i
0.0	343.791967	5.2887×10^{-1}	-2.0532×10
14.00	340.115764	5.2036×10^{-2}	2.0905×10
15.30	339.783264	2.8235×10^{-3}	-2.0934×10
15.40	**339.757748**	**-9.9634×10^{-4}**	**2.0937×10**
100	**320.751805**	**-1.8838**	**0**
262	**293.796058**	**-2.0258**	**0**
700	**248.552023**	**-2.3980**	**0**
1300	**211.731554**	**-2.8342**	**0**
2000	**184.082388**	**-3.2493**	**0**
3000	**161.082388**	**-4.2194**	**0**

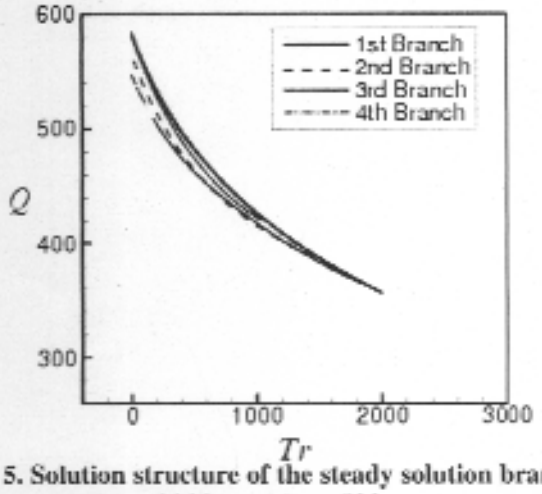

Fig. 5. Solution structure of the steady solution branches for $Dn = 2000$ and $Gr = 500$.

The first steady solution branch

The first steady solution branch for $Dn = 2000$ and $Gr = 500$ is solely depicted in Fig. 6(a) for $0 \le Tr \le 3000$. The branch starts from point a $(Tr = 0)$ and goes to the direction of increasing Tr as Q decreases which extends up to point d $(Tr = 2000)$ without any turning. Then, in order to observe the change of the flow patterns on the first branch, contours of typical secondary flow and temperature profile are drawn at several values of Tr as shown in Fig. 6 (b), where it is seen that the branch is composed of only two-vortex solutions. Three types of forces, *Coriolis force*, *strong centrifugal force* and *buoyancy force* act on the fluid particle at the same time, which make the flow patterns nearly symmetric. In the case of temperature profile, heat transmission from the outer wall to the fluid by convection becomes more frequent with the increase of rotation (Tr).

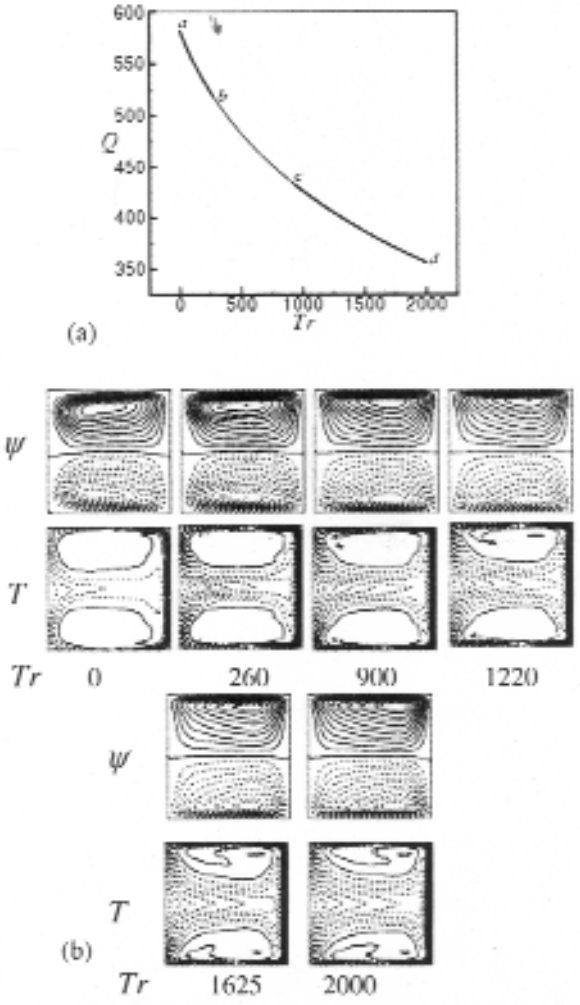

Fig. 6: (a) First steady solution branch with the region of linear stability for $Dn = 2000$ and $Gr = 500$. (b) Contours of secondary flow (top) and temperature profile (bottom) on the first steady solution branch at several values of Tr.

The Second steady solution branch

We draw the second steady solution branch for $Dn = 2000$ separately in Fig. 7(a). The branch has a similarity with the second branch obtained for $Dn = 1000$, and the only difference is that it extends up to larger Tr. As seen in Fig.7(a), the branch starts from point a $(Tr = 0)$ and goes to the direction of increasing Tr as Q decreases and arrives at point b $(Tr = 1400)$, where it turns to the opposite direction with a gentle turning at point b. The branch then goes to the direction of increasing Q and decreasing Tr up to point c $(Tr = 0)$.

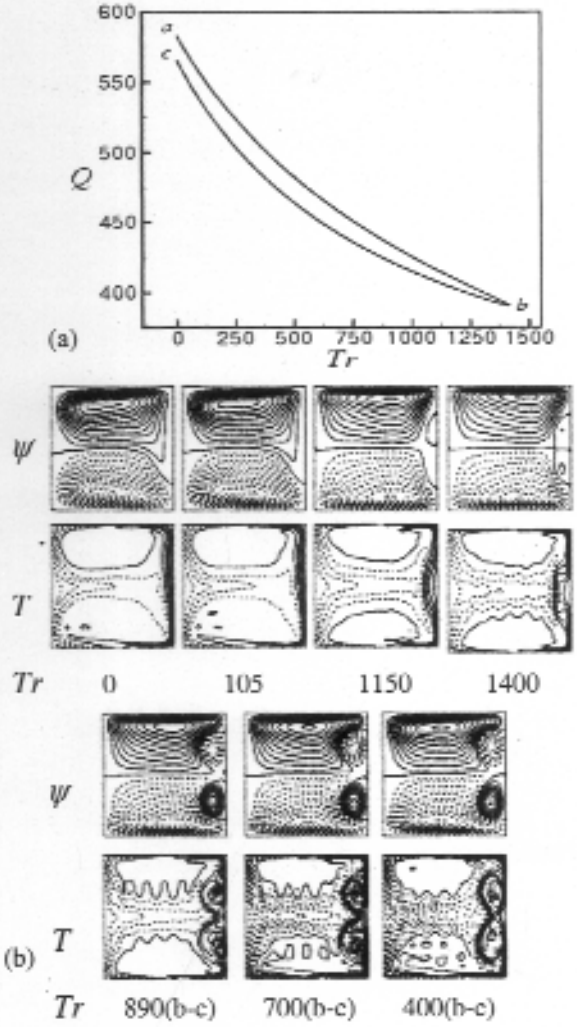

Fig. 7. (a) Second steady solution branch for $Dn = 2000$ and $Gr = 500$. (b) Contours of secondary flow (top) and temperature profile (bottom) for the second steady solution branch at different Tr (from upper branch to the lower)

To observe the change of the flow patterns, contours of typical secondary flow and temperature profile on this branch are shown in Fig. 7(b). It is found that the secondary flow is a two-vortex solution from point a to point b, but when the branch turns at point b down to point c the secondary flow becomes a perfect four-vortex solution.

The third steady solution branch

The third steady solution branch for $Dn = 2000$ is exclusively depicted in Fig. 8(a). As seen in Fig 8(a), the branch is very entangled with many turning points on its way, like the third branch obtained by Mondal *et al.* (2007) for the thermal flow for $Gr = 100$.

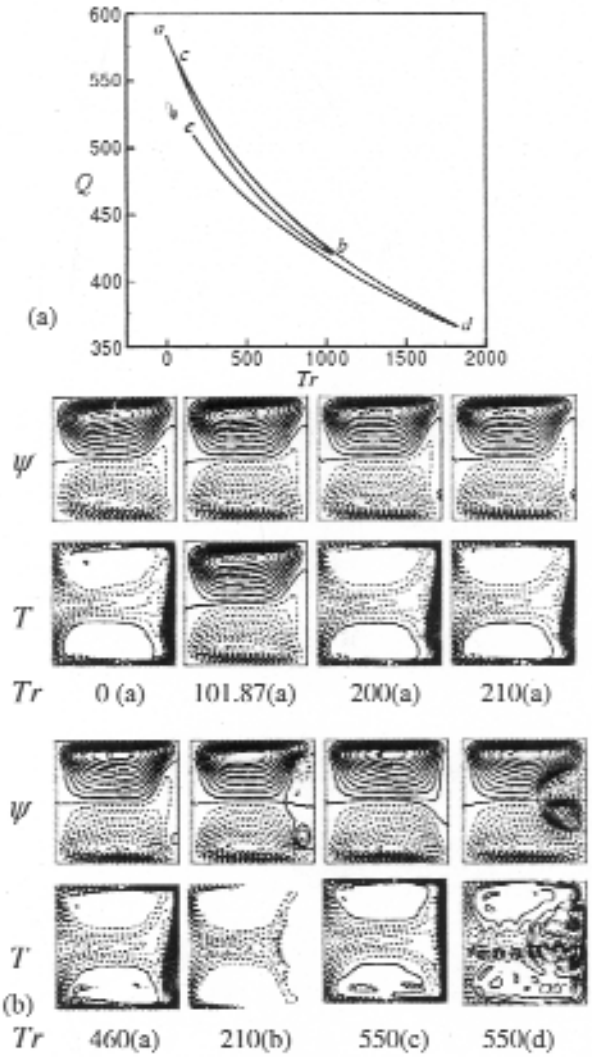

Fig. 8. (a) Third steady solution branch for $Dn = 2000$ and $Gr = 500$. (b) Contours of secondary flow and temperature profile (bottom) for the third steady solution branch at different values of Tr (from upper branch to the lower)

We draw the contours of secondary flow and temperature profiles at several values of Tr on this branch in Fig. 8(b), where it is observed that the branch consists of two- and four- vortex solutions, but they are different from those of the second steady solution branch.

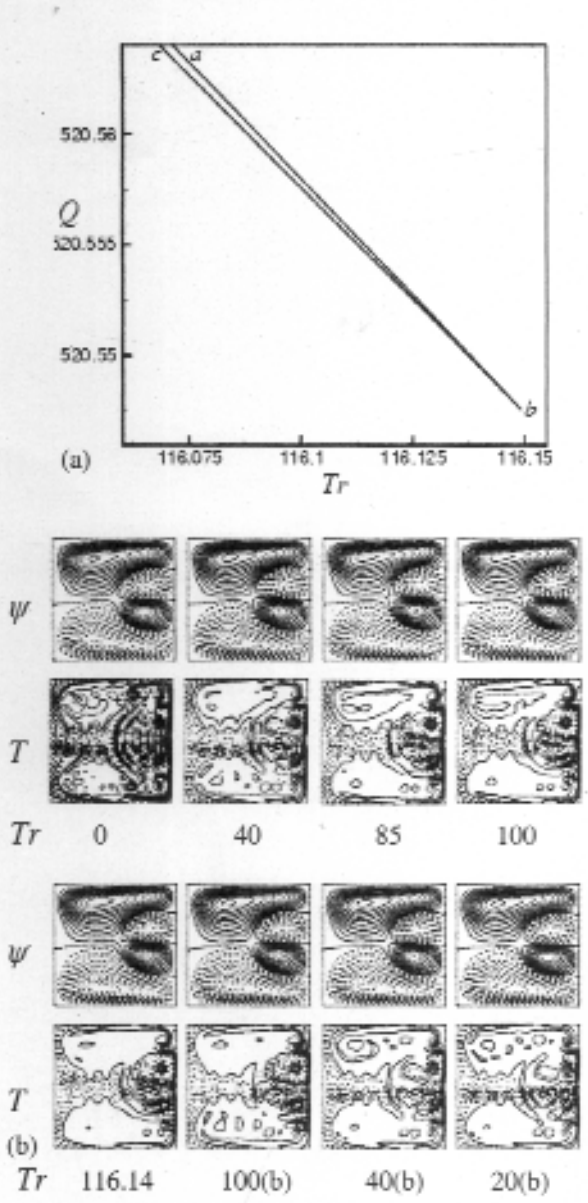

Fig. 9(a). Fourth steady solution branch for $Dn = 2000$ and $Gr = 500$. (b) Contours of secondary flow (top) and temperature profile (bottom) for the second steady solution branch at different values of Tr (from upper branch to the lower).

The Fourth steady solution branch

We draw the fourth steady solution branch for $Dn = 2000$, shown in Fig. 5 with thick solid purple line, is solely depicted in Fig. 9(a). An enlargement of this branch at point b is shown in Fig.9(b), in which we find that the branch has two parts very close to each other, the upper part (from point a to point b) and the lower part (from point b to from point c). The branch starts from point a and goes to the direction of increasing Tr and decreasing Q up to point $b(Tr = 116.14)$, where it experiences a reverse turning and goes to the direction of increasing Q as Tr decreases.

To observe the change of the flow patterns and temperature distributions, contours of typical secondary flow and temperature profile at several values of Tr on this branch are shown in Fig. 9(c), where it is seen that the branch is composed of asymmetric four-vortex solutions only. The temperature distribution is very vigorous as Tr increases.

Linear stability of the steady solution for $Dn = 2000$

We investigate linear stability of the steady solutions for $Dn = 2000$. It is found that among four branches of steady solutions only a portion of the first steady solution branch is linearly stable, while the other branches are linearly unstable.

Linear stability of the first steady solution branch for $Dn = 2000$ shows an interesting result. It is found that the branch is linearly stable in a couple of intervals of Tr, one for small Tr $(0 \le Tr \le 279)$ and another one for larger Tr $(922.90 \le Tr \le 3000)$. Thus the branch is linearly unstable for the region $(279.1 \le Tr \le 922.80)$. The eigenvalues of the first steady solution branch are shown in Table 2, where the eigenvalues with the maximum real part of σ (first eigenvalues) are presented. Those for the linearly stable solutions are written in bold letters. As seen in Table 2, the perturbation grows osciliatorily $(\sigma_i \neq 0)$ for $279 \le Tr \le 922.80$ and monotonically $(\sigma_i = 0)$ for $Tr \ge 922.80$. Therefore, the *Pitchfork bifurcation* occurs at $Tr = 279.10$ and the *Hopf bifurcation* at $Tr = 922.90$.

Table 2: Linear Stability of the first steady solution branch for $Dn = 2000$ and $Gr = 500$.

Tr	Q	σ_r	σ_i
0	**581.665065**	**-2.0525**	**0**
278.10	**517.278277**	**-3.1713×10^{-2}**	**8.7552×10**
279.00	**517.115175**	**-2.7722×10^{-4}**	**8.7596×10**
279.10	517.096957	3.2324×10^{-3}	8.7601×10
305.19	512.427375	8.8833×10^{-1}	8.8836×10
528.30	478.139438	5.5473×10^{0}	9.5355×10
922.80	433.296084	1.7839×10^{-3}	-9.4593×10
922.90	**433.286412**	**-1.8951×10^{-3}**	**-9.4591×10**
962.68	**429.491482**	**-1.5590×10^{0}**	**-9.3823×10**
1660	**375.904510**	**-3.2206×10^{0}**	**0**
2000	**356.047431**	**-3.4120×10^{0}**	**0**
3000	**322.417451**	**-4.1020×10^{0}**	**0**

Conclusions

In this study, a detailed numerical study on the solution structure and stability of flow through a rotating curved square duct has been performed by using the spectral method, and covering a wide range of the Taylor number, $0 \le Tr \le 3000$ and the Dean number $0 < Dn \le 3000$. A temperature difference is applied across the vertical sidewalls for the Grashof number $Gr = 500$, where the outer wall is heated and the inner one cooled. In the present study, two cases of the Dean numbers, $Dn = 1000$ and $Dn = 2000$ has been discussed in detail. In this study, a detailed numerical study on the solution structure and stability of flow through a rotating curved square duct has been performed by using the spectral method, and covering a wide range of the Taylor number, $0 \le Tr \le 3000$ and the Dean number $0 < Dn \le 3000$. A temperature difference is applied across the vertical sidewalls for the Grashof number $Gr = 500$, where the outer wall is heated and the inner one cooled. In the present study, two cases of the Dean numbers, $Dn = 1000$ and $Dn = 2000$ has been discussed in detail.

After a comprehensive survey over the parametric ranges, two branches of asymmetric steady solutions with two-, three- and four-vortex solutions are obtained for $Dn = 1000$. These vortices are generated due to the combined action of the *centrifugal force*, the *Coriolis force* and the *buoyancy force*. The first steady solution branch consists of asymmetric two-vortex solutions, while the second branch is composed of asymmetric two-, three- and four-vortex solutions. In the case of temperature transmission from the outer wall (heated wall) to the fluid, it is found that the convection becomes more frequent as the rotation increases. Linear stability of the steady solutions shows that between two branches of steady solutions only one branch (the first branch) is linearly stable while the other branch is unstable. It is found that the *Hopf bifurcation* occurs at the boundary between the stable and unstable solutions.

For $Dn = 2000$, on the other hand, we obtain four branches of asymmetric steady solutions. It is found that there exist two- and four- vortex solutions on various branches. Linear stability of the steady solutions shows that only the first branch is linearly stable in a couple of interval of the rotational parameter Tr, one for small Tr and another one for larger Tr, and thus the flow undergoes '*steady-stable* $\rightarrow$ *unstable* $\rightarrow$ *steady-stable*', if Tr is increased gradually. It is found that only two-vortex solutions are stable, while more than two-vortex solutions are linearly unstable.

References

Daskopoulos P and Lenhoff AM (1989), Flow in curved ducts: bifurcation structure for stationary ducts, *J. Fluid Mech.* **203**: 125–148.

Gottlieb D and Orazag SA (1977), Numerical Analysis of Spectral Methods, *Society for Industrial and Applied Mathematics*, Philadelphia, USA.

Ishigaki H (1993), Fundamental characteristics of laminar flows in a rotating curved pipe. *Trans. JSME*, **59-561-B**: 1494-1501.

Ishigaki H, (1996), Laminar flow in rotating curved pipes. *Journal of Fluid Mechanics*, **329:** 373-388.

Keller HB (1987), Lectures on Numerical Methods in Bifurcation Problems, *Springer*, Berlin.

Mondal RN (2006), Isothermal and Non-isothermal Flows Through Curved ducts with Square and Rectangular Cross Sections, *Ph.D. Thesis*, Department of Mechanical Engineering, Okayama University, Japan.

Mondal RN, Alam MM and Yanase S (2007), Numerical prediction of non- isothermal flows through a rotating curved duct with square cross section, *Thommasat Int. J. Sci and Tech.*, **12**(3): 24-43.

Selmi M. and Namdakumar K. and Finlay WH. (1994), A bifurcation study of viscous flow through a rotating curved duct, *J. Fluid Mechanics*, **262:** 353-375.

Selmi M. and Namdakumar K. (1999), Bifurcation Study of the Flow Through rotating Curved Ducts, *Physics of Fluids*, **11:** 2030-2043.

Wang, L. Q. and Cheng, K.C., (1996). Flow Transitions and combined Free and Forced Convective Heat Transfer in Rotating Curved Channels: the Case of Positive Rotation *Physics of Fluids*, **8:** 1553-1573.

Wang LQ and Yang TL (2004), Multiplicity and stability of convection in curved ducts: review and progress, *Adv. Heat Transfer*, **38**: 203–256.

Wang LQ and Liu F (2007a), Forced convection in slightly curved microchannels, *Int. J. Heat Mass Transfer*, **50**: 881–896.

Wang L and Liu F (2007b), Forced convection in tightly coiled ducts: Bifurcation in a high Dean number region, *International Journal of Non-Linear Mechanics*, **42**: 1018 – 1034

Winters KH (1987), A Bifurcation Study of Laminar Flow in a Curved Tube of Rectangular Cross-section, *Journal of Fluid Mechanics*, **180:** 343-369.

Yamamoto K, Yanase S and Alam MM (1999), Flow through a Rotating Curved Duct with Square Cross-section, *J. Phys. Soc.* Japan, **68:** 1173-1184.

Yang T and Wang L (2003), Bifurcation and Stability of Forced Convection in Rotating Curved Ducts of Square Cross Section, *Int. J. Heat Mass Transfer*, **46 :** 613-629.

Zhang JS, Zhang BZ and Jii J (2001), Fluid flow in a rotating curved rectangular duct. *Int. J. Heat and fluid flow*, **22:** 583-592.

Zhang JS, Shen XR and Zhang BZ (2000), The flow in rotating curved circular pipe. *J. Hydrodynam. Ser.* B **12** (1): 108-116.

Received: 02 June 2009; Revised: 02 March 2011; Accepted: 20 March 2011 .